RSC Advances

PAPER

View Article Online
View Journal | View Issue

Cite this: *RSC Adv.*, 2024, **14**, 3135

Catalytic hydrolysis of carbonyl sulfide in blast furnace gas over Sm-Ce-O_x@ZrO_2 catalyst†

Jintao Yu,‡[ac] Yao Lu,‡[ac] Sheng Wang,[b] Mutao Xu,[ae] Qijie Jin,[ae] Chengzhang Zhu,[a] Jisai Chen*[d] and Haitao Xu *[ae]

Received 14th October 2023
Accepted 9th January 2024

DOI: 10.1039/d3ra06833a

rsc.li/rsc-advances

Carbonyl sulfur (COS) is a prominent organic sulfur pollutant commonly found in the by-product gas generated by the steel industry. A series of Sm-doped CeO_x@ZrO_2 catalysts were prepared for the hydrolysis catalytic removal of COS. The results showed that the addition of Sm resulted in the most significant enhancement of hydrolysis catalytic activity. The 3% Sm_2O_3-Ce-O_x@ZrO_2 catalyst exhibited the highest activity, achieving a hydrolysis catalytic efficiency of 100% and H_2S selectivity of 100% within the temperature range of 90–180 °C. The inclusion of Sm had the effect of reducing the acidity of the catalyst while increasing weak basic sites, which facilitated the adsorption and activation of COS molecules at low temperatures. Appropriate doping of Sm proved beneficial in converting active surface chemisorbed oxygen into lattice oxygen, thereby decreasing the oxidation of intermediate products and maintaining the stability of the hydrolysis reaction.

1. Introduction

Carbonyl sulfide (COS) is widely present in the by-product gas (blast furnace gas, coke oven gas, converter gas) of the iron and steel industry.[1–3] Its acidity and polarity are weaker than H_2S, but its properties are more stable, making the removal of COS an important part of achieving gas fine desulfurization.[4,5] COS removal methods mainly include pyrolysis, hydrogenation, hydrolysis, chemical absorption and so on.[6,7] Pyrolysis is greatly affected by temperature, so the hydrogenation conversion method is widely used in industry, but the hydrogenation method requires higher temperature, and is prone to side reactions.[8–10] The catalytic hydrolysis method has high conversion efficiency and few side reactions. It is a hot research field at present and the core aspect is the research and development of hydrolysis catalysts.[11,12]

COS hydrolysis catalyst are based on γ-Al_2O_3, TiO_2, ZrO_2, *etc.*[13–16] The H_2S produced by hydrolysis is easily oxidised to monosulfur or further oxidised to sulphate, which is deposited on the surface of the catalyst, thus clogging up the holes of the catalyst.[17,18] γ-Al_2O_3 is strongly acidic, which reduces the surface alkalinity of aluminium-based catalysts, making the catalysts inadequate in low-temperature hydrolysis performance and stability.[19] In contrast, TiO_2 has stronger resistance to sulfate, and TiO_2 itself has better catalytic hydrolysis ability for COS, but the relatively small specific surface area of TiO_2 will limit its application to some extent.[20,21] Studies have shown that ZrO_2 has higher hydrolysis catalytic activity and stability than Al_2O_3 and TiO_2. Previous studies found that the hydrolysis activity of nano-TiO_2 and ZrO_2 is much higher than that of commercial nano-Al_2O_3, and that the increase in the activity is due to the decrease in surface hydrophilicity of the catalyst and increase in free surface basic hydroxyl groups.[22–24] However, the low-temperature hydrolysis activity of ZrO_2 was insufficient, and the loaded metal oxides were proved to be effective in enhancing the hydrolysis activity of the catalysts.[25,26] Consequently, the catalyst for the hydrolysis catalytic removal of carbonyl sulfur should be bifunctional, which means catalyst should have both ox-red and acid–base sites. Moreover, acid sites should be medium strength. One of the ways of such type catalyst's design is based on the application of oxide composites.

Alkali metals and alkaline earth metals regulate the alkali content and alkali strength distribution on the catalyst surface, but they do so in slightly different ways.[27,28] Alkali metals have a significant modulating effect on alkali content, while alkaline earth metals have a significant modulating effect on alkali strength. Rare earth elements such as La, Ce and Pr, which have a unique 4f electron layer structure, are used as excellent catalytic materials and co-catalysts, and they exhibit unique catalytic properties in chemical reactions. When they are used in

[a]*School of Environmental Science and Engineering, Nanjing Tech University, Nanjing 210009, PR China. E-mail: htxu@njtech.edu.cn*

[b]*State Key Laboratory for Clean and Efficient Coal-fired Power Generation and Pollution Control, State Key Laboratory of Low-carbon Smart Coal-fired Power Generation and Ultra-clean Emission, Nanjing 210046, China*

[c]*Shanghai Institute of Chemical Industry Environmental Engineering Co. Ltd, Shanghai 200333, PR China*

[d]*CCSC Nanjing Luzhou Environment Protection Co., Nanjing 211100, PR China*

[e]*Nanjing Gekof Institute of Environmental Protection Technology & Equipment Co. Ltd, Nanjing 210031, PR China*

† Electronic supplementary information (ESI) available. See DOI: https://doi.org/10.1039/d3ra06833a

‡ Jintao Yu and Yao Lu contributed equally.

combination with components such as metals or their oxides, they have obvious synergistic effects and show reaction activities that far exceed the expected ones.[29–32]

Consequently, this study utilized CeO_2 as the primary active component of the catalyst and ZrO_2 as the catalyst carrier. The aim was to evaluate various metal oxides (Sm, Y, Na, K) for doping modification. After screening the optimal metal oxides for doping, the doping amount was adjusted to determine the most effective ratio. The morphology and structure of the catalyst were characterized, and the reasons behind the improvement in hydrolysis catalytic efficiency and anti-poisoning ability were analyzed. Additionally, the preparation conditions and process parameters of the catalyst were investigated to determine the optimal ones.

2. Experimental

2.1 Catalyst preparation

In this experiment, a specific quantity of nano-ZrO_2 and $Ce(NO_3)_3 \cdot 6H_2O$ was carefully measured and placed in a beaker. Deionised water was then added to the mixture, followed by a certain amount of $Sm_2(NO_3)_3 \cdot 6H_2O$, $Y(NO_3)_3$, Na_2CO_3, and K_2CO_3, with a doping concentration of 1%. The mixture was stirred at a temperature of 80 °C for a duration of 8 h. The dried solid product was removed by spatula into a quartz crucible. Subsequently, the solid material was calcined in an air atmosphere at 600 °C for a period of 2 h, resulting in the formation of catalyst samples. These catalysts were given the names Sm-CeO_x@ZrO_2, Y-CeO_x@ZrO_2, Na-CeO_x@ZrO_2, and K-CeO_x@ZrO_2, respectively. Furthermore, additional catalyst samples were prepared by adjusting the amount of $Sm_2(NO_3)_3 \cdot 6H_2O$, resulting in different doping concentrations of Sm. These samples were designated as 1% Sm_2O_3-Ce-O_x@ZrO_2, 2% Sm_2O_3-Ce-O_x@ZrO_2, 3% Sm_2O_3-Ce-O_x@ZrO_2, 4% Sm_2O_3-Ce-O_x@ZrO_2, and 5% Sm_2O_3-Ce-O_x@ZrO_2. The detail qualification about the reagents was provided in ESI†.

2.2 Catalytic activity test and characterization

The detail information of characterization and catalytic activity test was provided in ESI†.

3. Results and discussion

3.1 Screening catalysts

In order to optimize the performance of catalyst, an investigation was conducted to examine the influence of doping with rare earth metals Sm and Y, as well as alkali metals Na and K. The experimental findings presented in Fig. 1 illustrated the COS conversion and H_2S selectivity of the 1% MO_x dopant on a 15% CeO_x@ZrO_2 catalyst. The results clearly demonstrated that, within the temperature range of 60 to 180 °C, the impact of rare earth metal doping on the hydrolysis performance of the catalyst surpassed that of alkali metals. Notably, Sm as a dopant exhibited the most substantial enhancement in the hydrolysis activity, achieving a hydrolysis efficiency of 100% at 180 °C. This positive outcome could be attributed to the reinforcement of the synergistic interaction between the active component of the catalyst and the carrier through the addition of Sm, resulting in an increased abundance of hydroxyl groups on the catalyst and ultimately enhancing the hydrolysis efficiency.[33]

3.2 Catalytic properties of Sm-based catalysts

Fig. 2 presented the performance of catalysts containing different amounts of Sm_2O_3-Ce-O_x@ZrO_2. The evaluation was based on COS conversion and H_2S selectivity. The findings indicated that the catalytic activity was most favorable when the doping amount of Sm_2O_3 constituted 3% of the carrier mass fraction. Specifically, the COS conversion of 3% Sm_2O_3-Ce-O_x@ZrO_2 is 13.7% higher than that of 1% Sm_2O_3-Ce-O_x@ZrO_2 at 60 °C. Moreover, the H_2S selectivity of 3% Sm_2O_3-Ce-O_x@ZrO_2 reaches 90.7% at 60 °C. This outcome was attributed to the enhanced synergistic effect among Sm, Ce, and Zr metals resulting from the increased doping amount of Sm.[34]

The dispersion state of the active component in the catalyst and the interaction between the active component and the carrier were greatly influenced by the calcination temperature, thus altering the catalytic activity of the catalyst.[35,36] Fig. 3 showed the curves of the COS hydrolysis conversion and H_2S selectivity for 3% Sm_2O_3-Ce-O_x@ZrO_2 catalysts calcined at different temperatures. The results indicated that the optimal

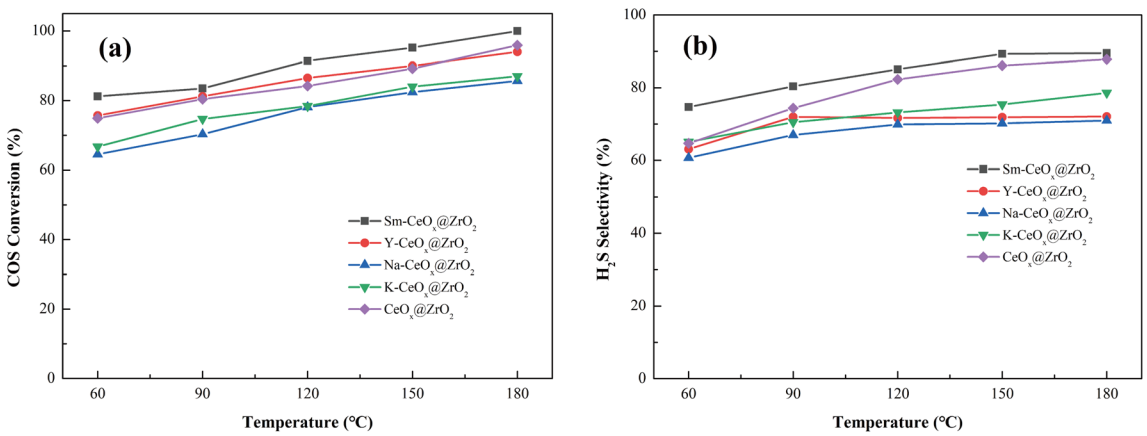

Fig. 1 (a) COS conversion, (b) H_2S selectivity of M-Ce-O_x@ZrO_2 catalysts.

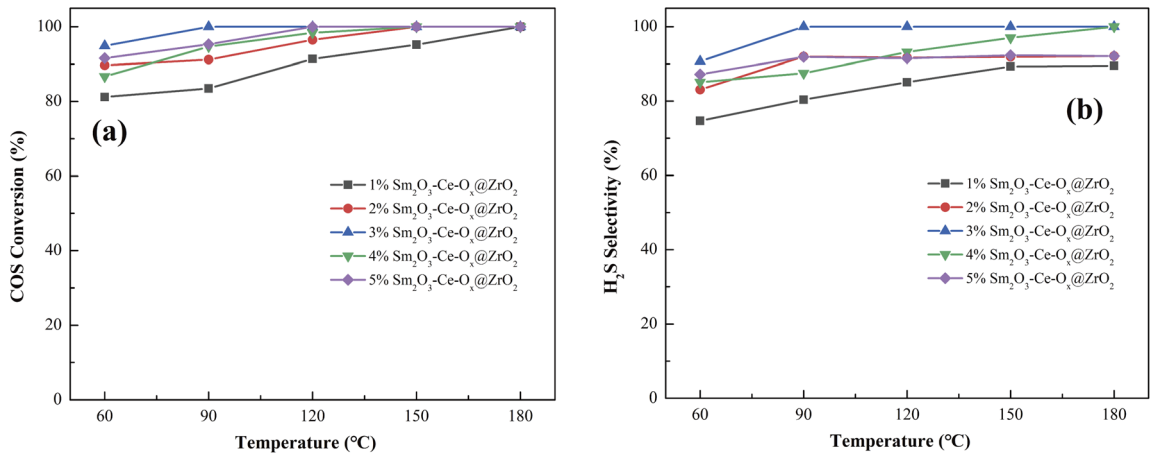

Fig. 2 (a) COS conversion, (b) H_2S selectivity of Sm-Ce-O_x@ZrO_2 catalysts with different Sm contents.

calcination temperature for the 3% Sm_2O_3-Ce-O_x@ZrO_2 catalyst was 600 °C. When the calcination temperature was increased from 300 °C to 600 °C, the COS conversion and H_2S selectivity of the 3% Sm_2O_3-Ce-O_x@ZrO_2 catalyst both increased. The COS conversion increased from 71.1% to 94.9%, and the H_2S selectivity increases from 71.7% to 90.7% at 60 °C. However, when the calcination temperature was 700 °C, the catalytic performance of the 3% Sm_2O_3-Ce-O_x@ZrO_2 catalyst decreased. This might be attributed to the fact that excessively high calcination temperatures were unfavorable for the dispersion of the active component on the catalyst surface, while also leading to the destruction of the catalyst structure, thereby resulting in a decrease in the catalytic performance of the catalyst.[37,38]

The calcination time of catalyst had an impact on both the COS conversion and H_2S selectivity of the catalyst. Fig. 4 illustrated the catalytic performance and H_2S selectivity of catalysts prepared with different calcination times at 600 °C. It can be observed that the hydrolysis activity of the catalyst first increased and then decreased with increasing calcination time. The optimal calcination time for the catalyst was 2 h, with a COS conversion of 94.9% at 60 °C and an H_2S selectivity of 90.7%. Compared to a calcination time of 1 h, the hydrolysis efficiency increased by 25.6% and the H_2S selectivity increased by 23.1%. The hydrolysis efficiency and H_2S selectivity both remained at 100% after 90 °C. This was because a too short calcination time cannot form a Sm-Ce-Zr solid solution, reducing the redox properties of the catalyst and subsequently affecting its acidity and basicity. With further prolongation of the calcination time, the COS conversion decreased to 82% at 60 °C when the calcination time was 3 h, and further decreased to 78.4% when the calcination time was 4 h. An excessively long calcination time led to a decrease in COS conversion and a corresponding decrease in H_2S selectivity, possibly due to the destruction of the pore structure caused by the prolonged calcination time, resulting in a decrease in hydrolysis activity.

3.3 Efficiency of Sm-based catalysts

The stability of catalyst was one of the factors used to evaluate the performance of a catalyst.[39,40] Fig. 5 illustrated the stability test results for different catalysts. From Fig. 1(a), it could be observed that the 3% Sm_2O_3-Ce-O_x@ZrO_2 catalyst exhibited the best stability, maintaining 90% hydrolysis efficiency even after continuous testing

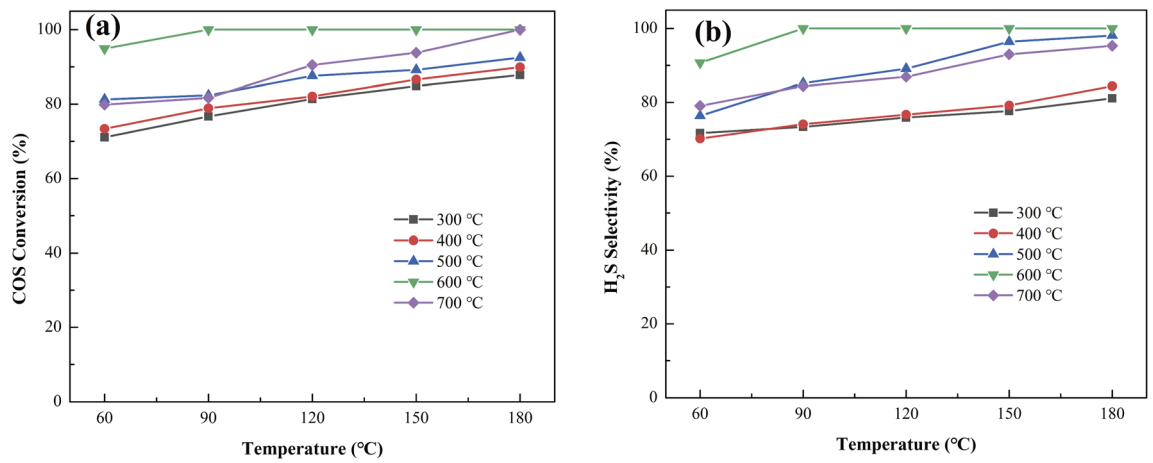

Fig. 3 (a) COS conversion, (b) H_2S selectivity of 3% Sm_2O_3-Ce-O_x@ZrO_2 catalysts under different calcination temperatures.

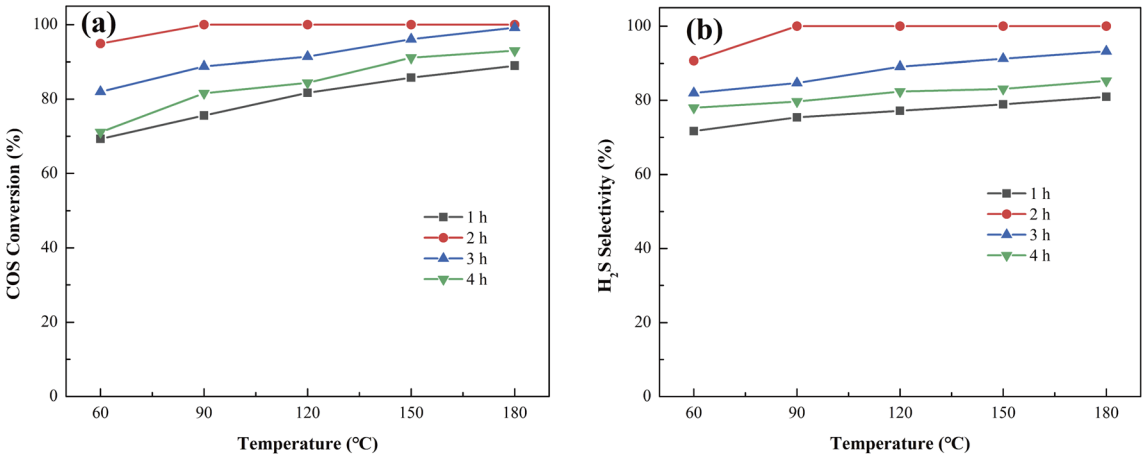

Fig. 4 (a) COS conversion, (b) H_2S selectivity and of 3% Sm_2O_3-Ce-O_x@ZrO_2 catalysts under different calcination time.

for 20 h. This indicated that the addition of Sm enhanced the stability of the CeO_x@ZrO_2 catalyst. Based on this, the stability of the 3% Sm_2O_3-Ce-O_x@ZrO_2 catalyst under different temperature conditions was investigated. Fig. 5(b) depicted the test curves for the 3% Sm_2O_3-Ce-O_x@ZrO_2 catalyst at three different temperatures: 60 °C, 90 °C, and 120 °C. It can be seen that the COS conversion rate dropped to 90% after continuous testing for 7 h at 60 °C. This might be attributed to the condensation of H_2O in the reaction gas, which covered the catalyst surface and reduced the hydrolysis activity. The catalyst maintained a 90% COS conversion for 30 h at 120 °C, which demonstrated the significant stability improvement of the catalyst with increased temperature.

The 3% Sm_2O_3-Ce-O_x@ZrO_2 catalyst demonstrated superior catalytic performance in COS hydrolysis at lower temperatures (<90 °C) compared to both Al-based catalysts and activated carbon series catalysts (Table 1). This suggested that the addition of Sm_2O_3 effectively enhanced the basicity of the catalyst surface, increasing the number of active sites. As a result, the catalyst was able to promote the conversion of COS to H_2S even at lower reaction temperatures, with the hydrolysis reaction playing a dominant role in the surface reaction.

3.4 Analysis of components

The X-ray diffraction patterns of different catalysts were presented in Fig. 6. From the graph, it can be observed that the catalysts exhibited diffraction peaks at $2\theta = 17.3°$, 24.1°, 28.2°, 31.5°, 34.1°, 35.2°, 38.5°, 40.8°, 46.2°, 50.5°, 54.2°, 55.6°, 59.9°, 63.1°, and 65.8°. These peaks corresponded to the crystal planes (001), (110), (−111), (111), (002), (−201), (120), (−112), (201), (−121), (221), (−311), (−203), (113), and (023) of ZrO_2 (PDF-ICDD 37-1484).[45,46] The diffraction peak at $2\theta = 47.5°$ corresponded to the crystal plane (220) of CeO_2 (PDF-ICDD 43-1002).[47] However, characteristic diffraction peaks of Sm_2O_3 were not observed in the XRD pattern of the catalysts. This could be due to the low mass fraction of Sm in the catalyst or the highly dispersed or amorphous nature of Sm_2O_3 on the catalyst surface.

3.5 Specific surface area analysis

The N_2 adsorption and desorption curves, pore size distribution, and specific surface area of five catalyst groups were shown in Fig. 7 and Table 2. According to Table 2, when the doping amount was 3%, the specific surface area of the catalyst Sm_2O_3-Ce-O_x@ZrO_2 increased from 27 $m^2\ g^{-1}$ to 30 $m^2\ g^{-1}$. The larger

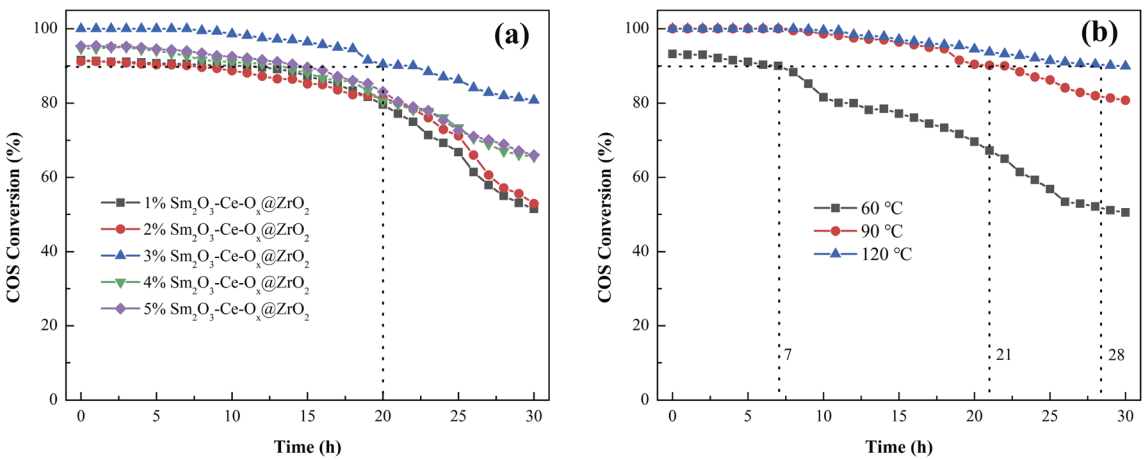

Fig. 5 Stability of Sm_2O_3-Ce-O_x@ZrO_2 catalyst: (a) different Sm contents, (b) different reaction temperature.

Table 1 The summary results of published catalysts performance

Catalyst	Concentration (ppm)	Temperature (°C)	GHSV (h^{-1})	Conversion (%)	Ref.
0.5% Pt/5% Ba/Al_2O_3	500–1000	200	7000	100	41
5% K/Mo-Al_2O_3	150	120	17 000	100	42
Fe_1Cu_4/AC	150	130	10 000	70	43
10Ni/AC	340	160	20 000	100	44

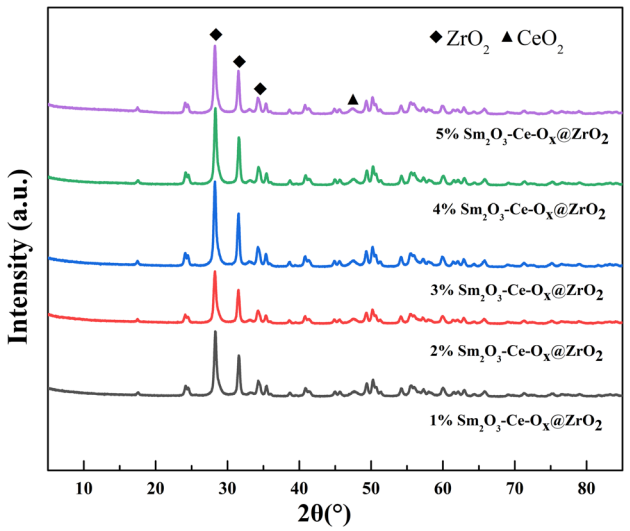

Fig. 6 XRD patterns of Sm_2O_3-Ce-O_x@ZrO_2 catalysts with different Sm contents.

specific surface area increased the effective contact area between the reactants and the catalyst, which was beneficial for the adsorption and diffusion of reactant molecules on the catalyst surface. Meanwhile, the number of active sites of the catalyst were increased, thereby enhancing the hydrolysis activity of the catalyst. Although the catalysts with different Sm additions had different average pore diameters, the average pore diameters of each catalyst were still much larger than the molecular dynamic diameters of COS (0.34 nm) and H_2O (0.27–0.32 nm), which suggests that COS and H_2O can enter the internal pores of the catalysts for hydrolysis reactions.[48]

3.6 Microscopic morphology analysis

SEM images of catalysts with different Sm contents were shown in Fig. 8. From Fig. 8(f), it can be observed that the catalysts composed of a series of irregular nanospheres, all of which exhibited irregular geometric shapes. Specifically, the 1% Sm_2O_3-Ce-O_x@ZrO_2 catalysts agglomerated together to form a block-like structure with a relatively large volume, thus exhibiting a smaller specific surface area. With increasing Sm doping level, the block-like structure of the catalysts became smaller and more numerous, resulting in an increased specific surface area. When the Sm_2O_3 doping level reached 3%, the catalyst surface was enriched with a large number of spherical particles, and more obvious large pores were observed between the particles.[49] When the Sm_2O_3 doping level reached 3%, the catalyst surface was enriched with a large number of spherical particles, and more obvious large pores were observed between the particles. The porous structure contributed to an increased specific surface area of the catalyst, which was also confirmed by BET test results. A larger specific surface area facilitated the adsorption and reaction of flue gas on the catalyst surface, leading to improved hydrolysis activity. However, the 5% Sm_2O_3-Ce-O_x@ZrO_2 catalysts exhibited a significantly increased block-like volume and reduced quantity.

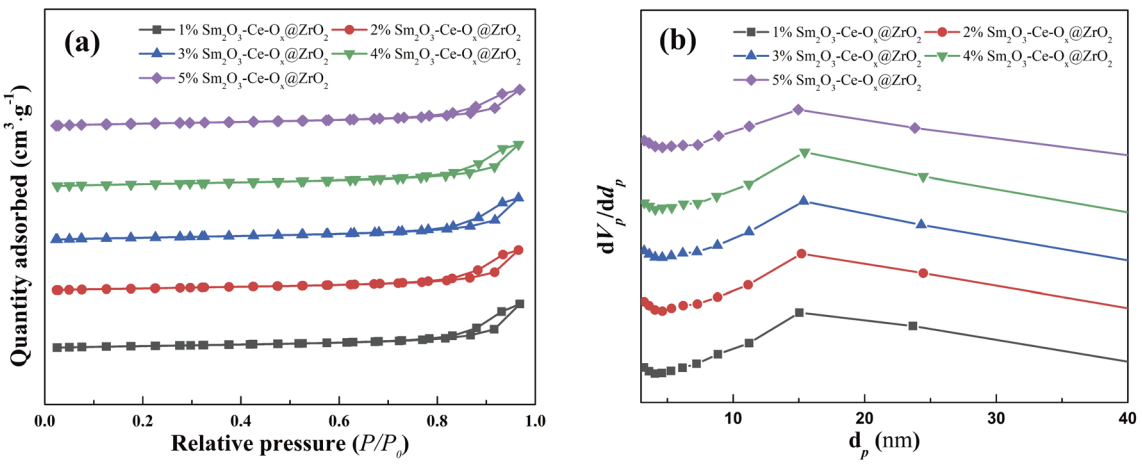

Fig. 7 (a) N_2 adsorption–desorption and (b) pore size distribution curves of Sm_2O_3-Ce-O_x@ZrO_2 catalysts with different Sm contents.

Table 2 Structural parameter of Sm_2O_3-Ce-O_x@ZrO_2 catalysts with Sm contents

Sample	BET surface area/(m^2 g^{-1})	Pore volume/(cm^3 g^{-1})	Average pore diameter/nm
1% Sm_2O_3-Ce-O_x@ZrO_2	27	0.10	15.6
2% Sm_2O_3-Ce-O_x@ZrO_2	27	0.10	14.1
3% Sm_2O_3-Ce-O_x@ZrO_2	31	0.10	13.2
4% Sm_2O_3-Ce-O_x@ZrO_2	30	0.100	13.2
5% Sm_2O_3-Ce-O_x@ZrO_2	33	0.09	10.9

3.7 Surface element composition analysis

The X-ray photoelectron spectroscopy (XPS) spectra of the Ce 3d, O 1s, and Zr 3d elements on different catalyst surfaces were depicted in Fig. 9. Fig. 9(a) illustrated the fitting curves of the Ce 3d peaks on different catalysts. The Ce 3d peaks can be divided into Ce^{3+} (902.7 eV and 885.1 eV) and Ce^{4+} (916.4 eV, 907.5 eV, 900.5 eV, 898.1 eV, 888.9 eV, 882.1 eV).[50] It can be observed that the intensity of the Ce 3d peaks remained relatively unchanged as the doping level increases. This might be due to the fact that the relative concentration of Sm in the catalyst did not increase significantly in terms of overall content. Furthermore, according to Table 3, the proportion of Ce^{3+} in the catalyst gradually decreased with increasing Sm doping. This was because the relative content of Ce^{3+} decreased and some Sm was embedded in the Ce lattice, altering the structure and morphology of cerium oxide and forming a samarium–cerium solid solution, thereby enhancing the catalytic redox performance.[51] The coexistence of Ce^{4+} and Ce^{3+} indicated a strong interaction between Ce and Sm, increasing the number of oxygen vacancies on the catalyst surface and promoting the redox cycling between Ce^{4+} and Ce^{3+}. Consequently, the Sm doping can enhance the catalytic activity for hydrolysis.

Fig. 9(b) presented the peak fitting curves of different catalysts in the O 1s region. All catalysts exhibited peaks at 531.7 eV and 529.6 eV, with the peak around 531.7 eV attributed to chemisorbed surface oxygen (O_α) and the peak around 529.6 eV

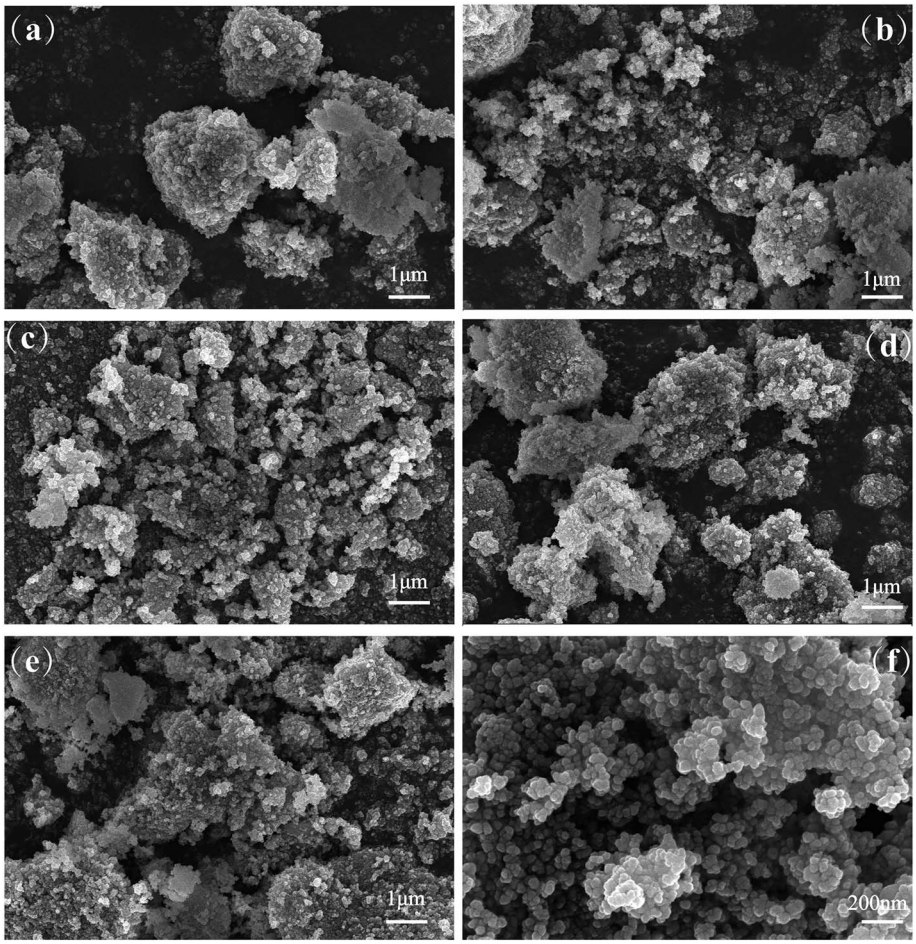

Fig. 8 SEM images of Sm_2O_3-Ce-O_x@ZrO_2 catalysts with Sm_2O_3 contents (a) 1%, (b) 2%, (c) 3%, (d) 4%, (e) 5%, (f) 5%–200 nm.

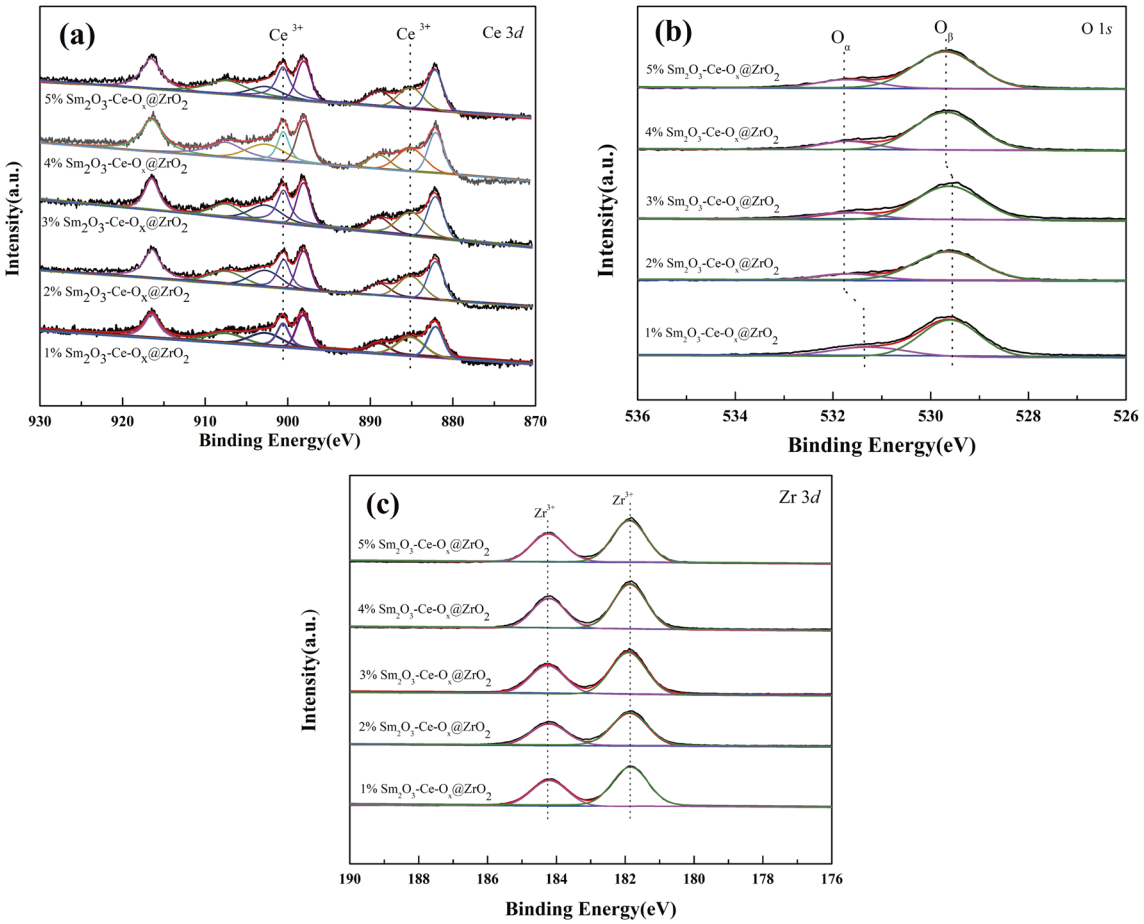

Fig. 9 XPS profiles of Sm_2O_3-Ce-O_x@ZrO_2 catalysts with different Sm contents (a) Ce 3d, (b) O 1s, (c) Zr 3d.

attributed to lattice oxygen (O_β).[52] With the introduction of Sm dopant, the O 1s spectral peaks shifted towards higher binding energies, indicating a strong interaction between Sm and O, which promoted catalytic activity. Chemisorbed surface oxygen was the most active oxygen species in catalytic reduction reactions, and studies had shown that oxygen adsorbed on the catalyst surface can oxidize intermediates generated during the hydrolysis of COS, leading to the formation of SO_4^{2-}. A large amount of sulfate species can poison the active sites on the catalyst surface, thereby impeding the long-term progress of the hydrolysis reaction. As shown in Table 3, the concentration of chemisorbed surface oxygen initially decreased and then increased with an increase in Sm doping concentration. When the doping level was 3%, the catalyst exhibited the lowest concentration of chemisorbed surface oxygen and the highest concentration of lattice oxygen. This indicated that appropriate Sm doping facilitated the conversion of active chemisorbed surface oxygen into more stable lattice oxygen, thereby reducing the oxidation of intermediate products and maintaining the stability of the hydrolysis reaction. This also explained the significant improvement in low-temperature hydrolysis activity and superior stability of the catalyst after Sm doping.

Fig. 9(c) displayed the fitted curves of the Zr 3d peaks for different catalysts. The binding energy of approximately 181.8 eV corresponds to the Zr $3d_{5/2}$ peak, while the binding energy of approximately 184.2 eV corresponds to the Zr $3d_{3/2}$ peak. It can be observed from the graph that the intensity of the Zr 3d spectral peaks decreases with an increase in the amount of Sm doping, possibly due to a decrease in the relative content of Zr in the catalyst.

3.8 Surface acid and alkaline analysis

NH_3-TPD is a commonly used characterization method to investigate the acidity of catalysts. The hydrolysis of COS was a base-catalyzed reaction, therefore, the stronger the acidity of the catalyst surface, the less favorable the adsorption of

Table 3 Atomic distribution of Sm_2O_3-Ce-O_x@ZrO_2 catalysts with different Sm contents

Sample	Ce^{3+}/Ce^{n+}	$O_\alpha/(O_\alpha + O_\beta)$	$O_\beta/(O_\alpha + O_\beta)$
1% Sm_2O_3-Ce-O_x@ZrO_2	0.257	0.249	0.751
2% Sm_2O_3-Ce-O_x@ZrO_2	0.254	0.167	0.833
3% Sm_2O_3-Ce-O_x@ZrO_2	0.244	0.151	0.849
4% Sm_2O_3-Ce-O_x@ZrO_2	0.238	0.161	0.839
5% Sm_2O_3-Ce-O_x@ZrO_2	0.185	0.183	0.817

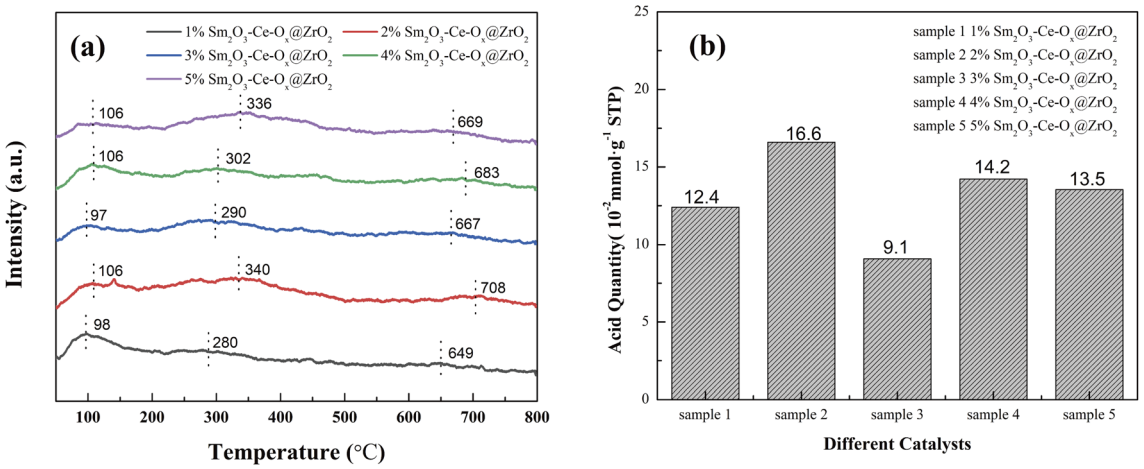

Fig. 10 (a) NH_3-TPD profiles and (b) acid quantity of Sm-Ce-O_x@ZrO_2 catalysts with different Sm contents.

reactants on the catalyst surface. Fig. 10 showed the NH_3-TPD test results of five groups of catalysts. All five groups of catalysts exhibited three NH_3 desorption peaks within the temperature range of 100 °C, around 300 °C, and 600–700 °C, which can be attributed to weak acid sites, medium-strong acid sites, and strong acid sites.[53] Among them, the desorption peak area of weak acid sites generally decreased with the increase of Sm doping amount. This indicated that the doping of Sm can effectively reduce the number of weak acid sites on the catalyst surface, making it easier for acidic reactants to adsorb on the catalyst surface, thereby improving the catalytic activity. The integrated peak area of medium-strong acid sites and strong acid sites was the smallest for the 3% Sm_2O_3-Ce-O_x@ZrO_2 catalyst, indicating the lowest acidity on the catalyst surface. The 3% Sm_2O_3-Ce-O_x@ZrO_2 catalyst had the lowest acid amount on the surface, which was beneficial for the adsorption and activation of COS molecules, thereby enhancing the catalytic activity of the catalyst for the hydrolysis of COS. Therefore, the 3% Sm_2O_3-Ce-O_x@ZrO_2 catalyst exhibited the highest catalytic activity for COS hydrolysis.

The enhancement of catalyst surface alkalinity was beneficial to the adsorption of COS molecules on the catalyst surface, thereby improving the catalytic activity of hydrolysis reaction. As shown in Fig. 11, two desorption peaks were observed for all five catalyst groups at around 90 °C and 300 °C. The desorption peak around 90 °C was attributed to weak alkaline sites, which were manifested by hydroxyl groups (–OH) on the oxide surface. The desorption peak around 300 °C was attributed to medium-strong alkaline sites, which were manifested by lattice oxygen on the oxide surface. It was believed that the active centers for COS hydrolysis were mainly weak alkaline centers. As clearly seen from the figure, the desorption peak area of weak alkaline sites was greater than that of medium-strong sites for all samples, indicating that the number of weak alkaline centers in the catalyst was greater than the number of medium-strong alkaline centers, which also confirmed that weak alkaline centers play a major role in catalytic activity. In addition, the peak intensity of weak alkaline sites increased with the increase of Sm loading, indicating that the doping of Sm effectively increased the number of weak alkaline centers in the catalyst and improved the catalytic efficiency of hydrolysis. Therefore, it can be concluded that the alkaline sites on the catalyst surface played a key role in the hydrolysis of COS.

3.9 Redox performance analysis

In order to investigate the redox performance of catalysts, the oxidation–reduction properties of five catalyst groups were characterized using H_2-TPR. The characterization test results of the five catalyst groups were shown in Fig. 12. All catalysts exhibited three hydrogen consumption peaks at around 380 °C, 510 °C and 660 °C. Firstly, the reduction peaks around 660 °C should be attributed to the bulk oxygen reductions of CeO_2.[54] Furthermore, the obvious shape changes reflected that the Sm doping had significant influence on the states of oxygen species. It is observed the shape changes of peaks around 380 and 510 °

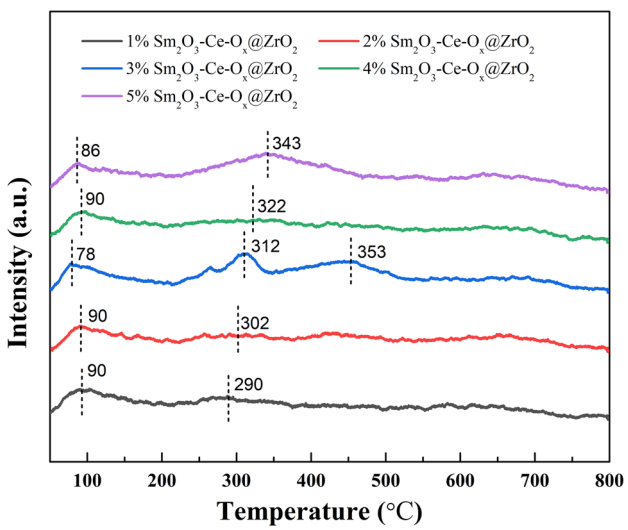

Fig. 11 CO_2-TPD profiles of Sm_2O_3-Ce-O_x@ZrO_2 catalysts with different Sm contents.

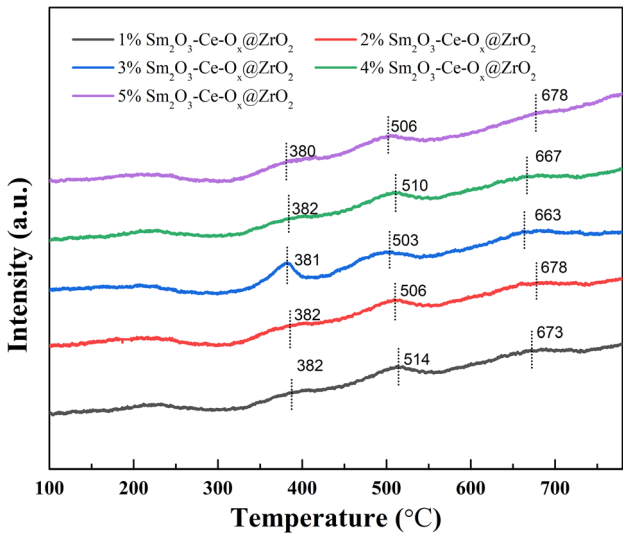

Fig. 12 H_2-TPR profiles of Sm_2O_3-Ce-O_x@ZrO_2 catalysts with different Sm contents.

C, the peak coming to an end beyond 600 °C, which represented that a small amount of oxygen species on the surface and in the bulk could be reduced in the catalysts. In other words, appropriate amount of Sm doping was conductive to promoting the evolution to the abundance subsurface oxygen species from the surface or in the bulk. The intensity of the hydrogen consumption peak around 380 °C showed an initial increase followed by a decrease. This can be attributed to the reduction of Sm species with different dispersion states on the ZrO_2 particles. When the Sm_2O_3 doping amount was 3%, the intensity of the hydrogen consumption peak reached its maximum. Additionally, the hydrogen consumption peak shifted to lower temperatures (from 514 °C to 503 °C). Notably, 3% Sm_2O_3-Ce-O_x@ZrO_2 catalyst exhibited the lowest reduction peak temperature and consumed more amount of hydrogen, indicating that doping Sm improved the redox performance of the catalyst. This was also one of the reasons why the 3% Sm_2O_3-Ce-O_x@ZrO_2 catalyst exhibited the best activity.

4. Conclusions

This study involved the selection of rare earth metals Sm and Y, as well as alkali metals Na and K, for doping in the CeO_x@ZrO_2 catalyst system. Results showed that when the doping amount of Sm_2O_3 reached 3%, the COS conversion and H_2S selectivity both reached 100% at 90 °C. The introduction of Sm_2O_3 led to an increase in the specific surface area of the catalyst and the enlargement of some of its pores. Consequently, the adsorption and activation of reactant molecules at low temperatures were affected. Additionally, the doping of Sm reduced the number of weak acid sites on the catalyst, while increasing the number of weak basic sites. This change proved beneficial for the adsorption and activation of COS molecules at low temperature. Proper doping of Sm facilitated the conversion of active surface chemisorbed oxygen into more stable lattice oxygen, thus decreasing the oxidation of intermediate products and maintaining the stability of the hydrolysis reaction.

Author contributions

Jintao Yu: data curation, formal analysis, roles/writing – original draft, Yao Lu: data curation, formal analysis, roles/writing – original draft, Sheng Wang: data curation, Mutao Xu: data curation, formal analysis, Qijie Jin: methodology, investigation, funding acquisition, Chengzhang Zhu: methodology, investigation, Jisai Chen: supervision, validation, project administration, Haitao Xu: supervision, validation; funding acquisition, project administration.

Conflicts of interest

The authors declare that there is no conflict of interests regarding the publication of this paper.

Acknowledgements

This work is supported by the National Key Research and Development Program of China (2021YFB3500600 and 2021YFB3500605), Natural Science Foundation of Jiangsu Province (BK20220365), Key R&D Program of Jiangsu Province (BE2022142), Natural Science Foundation of the Jiangsu Higher Education Institutions of China (22KJB610002), Science and Technology Plan of Yangzhou (YZ2022030, YZ2023020), Science and Technology Plan of Nanjing (202201019), Nanjing Science and Technology Top Experts Gathering Plan.

Notes and references

1 P. F. Li, G. C. Wang, Y. Dong, Y. Q. Zhuo and Y. M. Fan, A review on desulfurization technologies of blast furnace gases, *Curr. Pollut. Rep.*, 2022, **8**, 189–200.
2 Y. F. Wang, L. Ding, H. M. Long, J. J. Xiao, L. X. Qian, H. T. Wang and C. B. Xu, Carbonyl sulfur removal from blast furnace gas: Recent progress, application status and future development, *Chemosphere*, 2022, **307**, 136090.
3 X. Li, X. Q. Wang, L. L. Wang, P. Ning, Y. X. Ma, L. Zhong, Y. Wu and L. Yuan, Efficient removal of carbonyl sulfur and hydrogen sulfide from blast furnace gas by one-step catalytic process with modified activated carbon, *Appl. Surf. Sci.*, 2022, **579**, 152189.
4 K. Li, X. Song, T. T. Zhu, C. Wang, X. Sun, P. Ning and L. H. Tang, Mechanistic and kinetic study on the catalytic hydrolysis of COS in small clusters of sulfuric acid, *Environ. Pollut.*, 2018, **232**, 615–623.
5 J. Kim, J. Y. Do, K. Nahm, N.-K. Park, J. Chi, J.-P. Hong and M. Kang, Capturing ability for COS gas by a strong bridge bonding of a pair of potassium anchored on carbonate of activated carbon at low temperatures, *Sep. Purif. Technol.*, 2019, **211**, 421–429.
6 X. Sun, P. Ning, X. L. Tang, H. H. Yi, K. Li, D. He, X. M. Xu, B. Huang and R. Y. Lai, Simultaneous catalytic hydrolysis of carbonyl sulfide and carbon disulfide over Al_2O_3-K/CAC

catalyst at low temperature, *J. Energy Chem.*, 2014, **23**, 221–226.

7 X. Y. Kong, J. Ding, L. Xie, J. H. Qin and J. G. Wang, Lanthanum-bismuth mixed oxide catalyst with improved activity for carbonyl sulfide hydrolysis, *J. Environ. Chem. Eng.*, 2023, **11**, 109830.

8 L. Wang, F. Zhang and J. M. Chen, Carbonyl sulfide derived from catalytic oxidation of carbon disulfide over atmospheric particles, *Environ. Sci. Technol.*, 2001, **35**, 2543–2547.

9 G. C. Lei, Y. Zheng, Y. N. Cao, L. J. Shen, S. P. Wang, S. J. Liang, Y. Y. Zhan and L. L. Jiang, Deactivation mechanism of COS hydrolysis over potassium modified alumina, *Acta Phys.-Chim. Sin.*, 2023, **39**, 2210038.

10 X. Song, X. Chen, L. N. Sun, K. Li, X. Sun, C. Wang and P. Ning, Synergistic effect of Fe_2O_3 and CuO on simultaneous catalytic hydrolysis of COS and CS_2: Experimental and theoretical studies, *Chem. Eng. J.*, 2020, **399**, 125764.

11 X. Song, P. Ning, C. Wang, K. Li, L. H. Tang and X. Sun, Catalytic hydrolysis of COS over CeO_2 (110) surface: A density functional theory study, *Appl. Surf. Sci.*, 2017, **414**, 345–352.

12 P. Ning, X. Song, K. Li, C. Wang, L. H. Tang and X. Sun, Catalytic hydrolysis of carbonyl sulphide and carbon disulphide over Fe_2O_3 cluster: Competitive adsorption and reaction mechanism, *Sci. Rep.*, 2017, **7**, 14452.

13 Z. Wei, X. Zhang, F. L. Zhang, Q. Xie, S. Z. Zhao and Z. P. Hao, Boosting carbonyl sulfide catalytic hydrolysis performance over N-doped Mg-Al oxide derived from MgAl-layered double hydroxide, *J. Hazard. Mater.*, 2021, **407**, 124546.

14 C. M. Li, S. Y. Zhao, X. L. Yao, L. He, S. M. Xu, X. B. Shen and Z. L. Yao, The catalytic mechanism of intercalated chlorine anions as active basic sites in MgAl-layered double hydroxide for carbonyl sulfide hydrolysis, *Environ. Sci. Pollut. Res.*, 2022, **29**, 10605–10616.

15 E. C. Rupp, E. J. Granite and D. C. Stanko, Catalytic formation of carbonyl sulfide during warm gas clean-up of simulated coal-derived fuel gas with Pd/gamma-Al_2O_3 sorbents, *Fuel*, 2012, **92**, 211–215.

16 P. Ning, K. Li, H. H. Yi, X. L. Tang, J. H. Peng, D. He, H. Y. Wang and S. Z. Zhao, Simultaneous catalytic hydrolysis of carbonyl sulfide and carbon disulfide over modified microwave coal-based active carbon catalysts at low temperature, *J. Phys. Chem. C*, 2012, **116**, 17055–17062.

17 H. Y. Wang, H. H. Yi, X. L. Tang, P. Ning, L. Yu, D. He, S. Z. Zhao and K. Li, Catalytic hydrolysis of COS over calcined CoNiAl hydrotalcite-like compounds modified by cerium, *Appl. Clay Sci.*, 2012, **70**, 8–13.

18 A. Usmani, B. Tharat, A. Watwiangkham, N. Grisdanurak and S. Suthirakun, Enhancing kinetics of carbonyl sulfide hydrolysis using Pt-supported Al_2O_3 catalysts: first-principles-informed energetic span analysis, *J. Phys. Chem. C*, 2023, **127**, 9002–9012.

19 E. Sasaoka, K. Taniguchi, A. Uddin, S. Hirano, S. Kasaoka and Y. Sakata, Characterization of reaction between ZnO and COS, *Ind. Eng. Chem. Res.*, 1996, **35**, 2389–2394.

20 X. Song, P. Ning, C. Wang, K. Li, L. H. Tang, X. Sun and H. T. Ruan, Research on the low temperature catalytic hydrolysis of COS and CS_2 over walnut shell biochar modified by Fe-Cu mixed metal oxides and basic functional groups, *Chem. Eng. J.*, 2017, **314**, 418–433.

21 S. Z. Zhao, D. J. Kang, Y. P. Liu, Y. F. Wen, X. Z. Xie, H. H. Yi and X. L. Tang, Spontaneous formation of asymmetric oxygen vacancies in transition-metal-doped CeO_2 nanorods with improved activity for carbonyl sulfide hydrolysis, *ACS Catal.*, 2020, **10**, 11739–11750.

22 A. Aboulayt, F. Mauge, P. E. Hoggan and J. C. Lavalley, Combined FTIR reactivity and quantum chemistry investigation of COS hydrolysis at metal oxide surfaces used to compare hydroxyl group basicity, *Catal. Lett.*, 1996, **39**, 213–218.

23 Y. H. Yue, X. P. Zhao, W. M. Hua and Z. Gao, Nanosized titania and zirconia as catalysts for hydrolysis of carbon disulfide, *Appl. Catal., B*, 2003, **46**, 561–572.

24 J. West, B. P. Williams, N. Young, C. Rhodes and G. J. Hutchings, Low temperature hydrolysis of carbonyl sulfide using gamma-alumina catalysts, *Catal. Lett.*, 2001, **74**, 111–114.

25 O. Y. Gutierrez, C. Kaufmann and J. A. Lercher, Synthesis of methanethiol from carbonyl sulfide and carbon disulfide on (Co)K-promoted sulfide Mo/SiO_2 catalysts, *ACS Catal.*, 2011, **1**, 1595–1603.

26 S. Z. Zhao, H. H. Yi, X. L. Tang and C. Y. Song, Low temperature hydrolysis of carbonyl sulfide using Zn-Al hydrotalcite-derived catalysts, *Chem. Eng. J.*, 2013, **226**, 161–165.

27 X. Li, X. Q. Wang, L. L. Wang, L. Yuan, Y. X. Ma, Y. B. Xie, Y. R. Xiong and P. Ning, Alkali-induced metal-based coconut shell biochar for efficient catalytic removal of H_2S at a medium-high temperature in blast furnace gas with significantly enhanced S selectivity, *Sep. Purif. Technol.*, 2023, **306**, 122698.

28 J. N. Gu, J. X. Liang, S. J. Hu, Y. X. Xue, X. Min, M. M. Guo, X. F. Hu, J. P. Jia and T. H. Sun, Enhanced removal of COS from blast furnace gas via catalytic hydrolysis over Al_2O_3-based catalysts: Insight into the role of alkali metal hydroxide, *Sep. Purif. Technol.*, 2022, **295**, 121356.

29 P. T. Gao, Y. R. Li, Y. T. Lin, L. P. Chang and T. Y. Zhu, Promoting effect of Fe/La loading on gamma-Al_2O_3 catalyst for hydrolysis of carbonyl sulfur, *Environ. Sci. Pollut. Res.*, 2022, **29**, 84166–84179.

30 S. Z. Zhao, H. H. Yi, X. L. Tang, P. Ning, H. Y. Wang and D. He, Effect of Ce-doping on catalysts derived from hydrotalcite-like precursors for COS hydrolysis, *J. Rare Earths*, 2010, **28**, 329–333.

31 G. Y. Mu, Y. Zeng, Y. Zheng, Y. N. Cao, F. J. Liu, S. J. Liang, Y. Y. Zhan and L. L. Jiang, Oxygen vacancy defects engineering on Cu-doped Co_3O_4 for promoting effective COS hydrolysis, *Green Energy Environ.*, 2023, **8**, 831–841.

32 Y. Q. Zhang, Z. B. Xiao and J. X. Ma, Hydrolysis of carbonyl sulfide over rare earth oxysulfides, *Appl. Catal., B*, 2004, **48**, 57–63.

33 X. Z. Li, Z. L. Hu, X. B. Zhao and X. W. Lu, $Ce_{1-x}Sm_xO_2$-delta-attapulgite nanocomposites: synthesis via simple microwave approach and investigation of its catalytic activity, *J. Rare Earths*, 2013, **31**, 1157–1162.

34 P. F. Wang, J. Wang, J. Shi, X. Du, X. G. Hao, B. Tang, A. Abudula and G. Q. Guan, Low content of samarium doped CeO_2 oxide catalysts derived from metal organic framework precursor for toluene oxidation, *Mol. Catal.*, 2020, **492**, 111027.

35 J. Ashok and S. Kawi, Steam reforming of toluene as a biomass tar model compound over CeO_2 promoted Ni/CaO-Al_2O_3 catalytic systems, *Int. J. Hydrogen Energy*, 2013, **38**, 13938–13949.

36 N. Wang, K. Shen, L. H. Huang, X. P. Yu, W. Z. Qian and W. Chu, Facile route for synthesizing ordered mesoporous Ni-Ce-Al oxide materials and their catalytic performance for methane dry reforming to hydrogen and syngas, *ACS Catal.*, 2013, **3**, 1638–1651.

37 J. Yang, S. Ren, T. S. Zhang, Z. H. Su, H. M. Long, M. Kong and L. Yao, Iron doped effects on active sites formation over activated carbon supported Mn-Ce oxide catalysts for low-temperature SCR of NO, *Chem. Eng. J.*, 2020, **379**, 122398.

38 X. Fang, Y. J. Liu, Y. Cheng and W. L. Cen, Mechanism of Ce-modified birnessite-MnO_2 in promoting SO_2 poisoning resistance for low-temperature NH_3-SCR, *ACS Catal.*, 2021, **11**, 4125–4135.

39 Z. M. Liu, J. Z. Zhu, J. H. Li, L. L. Ma and S. I. Woo, Novel Mn-Ce-Ti mixed-oxide catalyst for the selective catalytic reduction of NO_x with NH_3, *ACS Appl. Mater. Interfaces*, 2014, **6**, 14500–14508.

40 X. B. Zhu, X. Gao, R. Qin, Y. X. Zeng, R. Y. Qu, C. H. Zheng and X. Tu, Plasma-catalytic removal of formaldehyde over Cu-Ce catalysts in a dielectric barrier discharge reactor, *Appl. Catal., B*, 2015, **170**, 293–300.

41 K. Nimthuphariyha, A. Usmani, N. Grisdanurak, E. Kanchanatip, M. Yan, S. Suthirakun and S. Tulaphol, Hydrolysis of carbonyl sulfide over modified Al_2O_3 by platinum and barium in a packed-bed reactor, *Chem. Eng. Commun.*, 2021, **208**, 539–548.

42 R. Cao, P. Ning, X. Q. Wang, L. L. Wang, Y. X. Ma, Y. B. Xie, H. Zhang and J. X. Qu, Low-temperature hydrolysis of carbonyl sulfide in blast furnace gas using Al_2O_3-based catalysts with high oxidation resistance, *Fuel*, 2022, **310**, 122295.

43 H. H. Han, Z. H. Zhang and Y. L. Zhang, Research on the catalytic hydrolysis of COS by Fe-Cu/AC catalyst and its inactivation mechanism at low temperature, *ChemistrySelect*, 2022, **7**, e202200194.

44 H. H. Yi, C. C. Du, X. D. Zhang, S. Z. Zhao, X. Z. Xie, L. L. Miao and X. L. Tang, Inhibition of CO in blast furnace flue gas on poisoning and deactivation of a Ni/Activated carbon catalyst in COS hydrolysis, *Ind. Eng. Chem. Res.*, 2021, **60**, 18183–18193.

45 P. Gao, F. Li, H. J. Zhan, N. Zhao, F. K. Xiao, W. Wei, L. S. Zhong, H. Wang and Y. H. Sun, Influence of Zr on the performance of Cu/Zn/Al/Zr catalysts via hydrotalcite-like precursors for CO_2 hydrogenation to methanol, *J. Catal.*, 2013, **298**, 51–60.

46 C. Z. Sun, H. Liu, W. Chen, D. Z. Chen, S. H. Yu, A. N. Liu, L. Dong and S. Feng, Insights into the Sm/Zr co-doping effects on N_2 selectivity and SO_2 resistance of a MnO_x-TiO_2 catalyst for the NH_3-SCR reaction, *Chem. Eng. J.*, 2018, **347**, 27–40.

47 N. Daelman, M. Capdevila-Cortada and N. Lopez, Dynamic charge and oxidation state of Pt/CeO_2 single-atom catalysts, *Nat. Mater.*, 2019, **18**, 1215–1221.

48 N.-K. Park, J. Y. Park, T. J. Lee, J.-I. Baek and C. K. Ryu, Catalytic reduction of SO_2 over Sn-Zr based catalysts for DSRP under high pressure, *Catal. Today*, 2011, **174**, 46–53.

49 X. M. Sun, W. J. Huang, L. P. Ji, H. M. Xu, Z. Qu and N. Q. Yan, Establishing a self-supporting system of H_2S production from SO_2 with induced catalytic reduction process for mercury capture with super-large enrichment, *Chem. Eng. J.*, 2023, **459**, 141493.

50 J. L. Wang, J. G. Li, C. J. Jiang, P. Zhou, P. Y. Zhang and J. G. Yu, The effect of manganese vacancy in birnessite-type MnO_2 on room-temperature oxidation of formaldehyde in air, *Appl. Catal., B*, 2017, **204**, 147–155.

51 Y. Lu, Q. J. Jin, W. Y. Ji, C. Z. Zhu, M. T. Xu, Y. Y. Zhu and H. T. Xu, Resource utilization of high concentration SO_2 for sulfur production over La-Ce-O_x@ZrO_2 composite oxide catalyst, *J. Rare Earths*, 2023, **41**(12), 1945–1952.

52 Q. J. Jin, M. M. Chen, X. J. Tao, B. X. Lu, J. Y. Shen, Y. S. Shen and Y. W. Zeng, Component synergistic catalysis of Ce-Sn-W-Ba-O_x/TiO_2 in selective catalytic reduction of NO with ammonia, *Appl. Surf. Sci.*, 2020, **512**, 145757.

53 S. Das, J. M. Dowding, K. E. Klump, J. F. McGinnis, W. Self and S. Seal, Cerium oxide nanoparticles: applications and prospects in nanomedicine, *Nanomedicine*, 2013, **8**, 1483–1508.

54 L. L. Zhao, Z. P. Zhang, Y. S. Li, X. S. Leng, T. R. Zhang, F. L. Yuan, X. Y. Niu and Y. J. Zhu, Synthesis of Ce_aMnO_x hollow microsphere with hierarchical structure and its excellent catalytic performance for toluene combustion, *Appl. Catal., B*, 2019, **245**, 502–512.